Nonlinear Dyn (2014) 76:1365–1377
DOI 10.1007/s11071-013-1215-y

ORIGINAL PAPER

Nonlinear vibration and dynamics of ceramic on ceramic artificial hip joints: a spatial multibody modelling

Ehsan Askari · Paulo Flores · Danè Dabirrahmani · Richard Appleyard

Received: 31 October 2013 / Accepted: 21 December 2013 / Published online: 21 January 2014
© Springer Science+Business Media Dordrecht 2014

Abstract The present study investigates nonlinear vibration and dynamic behaviour of a ceramic-on-ceramic hip implant. The aim of this research is to firstly gain a better understanding of hip squeaking and vibration and secondly to investigate the effect of friction on contact point path during normal gait. For this purpose, a spatial multibody dynamic hip model was developed, using a friction-velocity constitutive law combined with a Hertzian contact model. Furthermore, the physiological three-dimensional rotation angles and forces are taken into account to calculate tangential and normal contact forces, respectively. Comparing the outcomes with that available in the literature allowed for the validation of our approach. It was shown that the cause of hip squeaking is friction-induced vibration owing to different phenomena such as stick–slip friction, negative-sloping friction and contact force changes. Moreover, friction-induced vibration does significantly change contact point path during the gait when compared to non-friction analysis.

E. Askari (✉) · D. Dabirrahmani · R. Appleyard
Australian School of Advanced Medicine, Macquarie University, Sydney, NSW, Australia
e-mail: ehsanaskary@gmail.com

E. Askari · P. Flores
Department of Mechanical Engineering, School of Engineering, University of Minho, Campus de Azurém, 4800-058 Guimarães, Portugal

Keywords Nonlinear vibration and dynamics · Spatial multibody dynamic · Friction-induced vibration · Hip squeaking · Contact point track

1 Introduction

Ceramic-on-ceramic (CoC) hip arthroplasty has demonstrated very good clinical performance due to the superior wear resistance and low biological reactivity. However, the occurrence of audible squeaking in some patients is a cause for concern. In fact, the prevalence of hip squeaking is reported between 1 and 20% [1]. In vivo CoC fundamental squeaking frequencies have been measured in the range of 400–7500 Hz [2]. A possible cause of squeaking in metal-on-metal and CoC bearings without lubrication is the stick–slip phenomenon between the head and cup of artificial hip joints [3,4]. It has been computationally and experimentally shown that friction-induced vibration was the main reason of hip squeaking [5,6]. In order to consider this issue numerically, a complex eigenvalue method was employed to identify the stability properties of hip implants under laboratory conditions and in a pseudo-in vivo configuration. However, considerable differences between theoretical and in vivo results were observed, which could be associated with the choice of boundary conditions [7,8]. This study also reported that hip prostheses become unstable when the friction coefficient between components reaches critical values. It was concluded that increasing the critical friction

coefficient could decrease the occurrence of ceramic bearing squeaking [7,8]. Weiss et al. [9] found experimentally that there was oscillation behaviour on top of the gross head movement against the liner. This was a micrometre scale elliptical motion inside the liner and the vibrational pattern of hip implants was two dimensional. However, the hip squeaking frequencies they reported were higher than those found in vivo.

It is known that when two surfaces slide against each other, friction develops and acts as a resistance to relative motion. Sliding is an unsteady phenomenon made up of continuous or transient contact resulting in intermittent or cyclical squeaking due to a slight variation in the normal contact load for instance [10]. Moreover, friction force acts like a cross-coupling force linking normal and parallel motions at the contact surface [11]. It is well known that friction can induce vibration in structures owing to instability in the structural system such as the instability due to a surface property for which friction decreases as relative velocity between sliding surfaces increases [5,10]. Moreover, there are other sources of instability in structure systems, namely mode-coupling, Sprag-slip, frictional follower forces, stick–slip and material nonlinearity that have all been suggested as possible causes of self-excited friction-induced vibration [5,10–13].

In addition to the short-time frame dynamic effects described above, friction is also affected by longer time frame parameters such as deformation and wear of surfaces. Hence, to update the wear and deformation, the wear process on the hip implant surfaces should be calculated over time. One of the most important parameters to predict wear between the femoral head and cup is the slide track shape as any variation in its shape can cause a huge variation in the wear rate [14–16]. Mattei et al. [17] developed a theoretical contact point track to compute wear which assumed that the reaction force between the head and cup lies in the direction joining their centres due to frictionless contact [18]. Another technique to determine wear was fixing the centre of the femoral head and then simulating physiological rotations of the femur by applying physiological rotations [19]. Furthermore, Ramamuri et al. [20] provided loci of movement of selected points on the femoral head during normal gait computationally. Saikko and Calonius [21] developed a computational method based on Euler angles, and utilised it to compute slide tracks for the three-axis motion of the hip joint during walking and for two hip simulators. The slide track patterns resulting from the gait waveforms were found to be similar to those produced by hip simulators. Sariali et al.[22] also provided sliding path of motion between the head and cup when the hip implant is in edge loading or in normal centred conditions using Leeds II hip simulator.

The aims of the present paper were firstly to investigate the effect of friction on the femoral head/liner sliding track shape and secondly gain a better understanding of friction-induced vibration in artificial hip joints. This desideratum is achieved by developing the planar multibody dynamic model proposed by Askari et al. [23] to analysis three-dimensional vibration and dynamics of artificial hip joints. The friction-induced vibration and contact-impact events occurring between the head and cup surfaces were taken into consideration as external generalised hip forces in the governing equation of the motion. A friction-velocity relation [24] and a Hertz contact model [25] were employed to formulate tangential and normal contact forces, respectively. Physiological rotation angles and forces were also taken into account. Nonlinear governing motion equations were solved, using adaptive Runge-Kutta-Fehlberg method. In addition, a FFT frequency analysis of the audible sounds from CoC hip acceleration was carried out to assess the frequency of hip squeaking. This approach is verified by comparing outcomes with in vivo, experimental and computational results available in the literature. The effect of hip implant size on hip squeaking frequencies and friction on both contact stress/moments and squeaking of hip implants were also analysed as well as the path shape of contact point between the cup and head. Finally, friction-induced vibration of artificial hip joints owing to stick–slip, negative-sloping friction, contact force changes and friction follower force was analysed.

2 Multibody dynamic approach

2.1 Description of the artificial hip joint model

In this section, a mathematical model of an artificial hip joint is presented as a spatial multibody system. When the joint is assumed to be ideal, the femoral head moves without friction having three relative rotational degrees-of-freedom, while the femoral head centre translation is constrained. However, the presence of head/liner clearance results in a six-degrees-of-

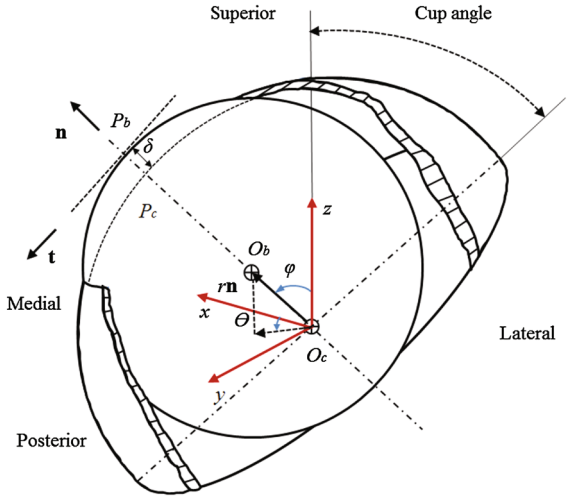

Fig. 1 A representation of the head/cup articulation

freedom unconstrained system exhibiting translational and rotational movement. The vibrational dynamics of this system are controlled by contact-impaction forces generated when the femoral head and cup liner collide. Thus, this type of system can be referred to as a force joint, since it deals with force constraints instead of kinematic constraints [26–32].

Let's consider a head/cup couple of an artificial hip joint, depicted in Fig. 1, in which the femoral head is separated from the femoral stem and neck through the cross-section proposed in Askari et al. [23] for the case of planar systems. Pc and Pb denote potential contact points located on the femoral head and cup surfaces. These points reside on the plane of collision, which is represented by a plane tangential to both the ball and cup surfaces at the contact point. The femoral head centre with respect to the reference coordinate system is defined by three coordinates (r, θ, φ). The radial clearance size is defined as $c = R_c - R_b$, where R_c and R_b denote the cup and femoral radius, respectively. The penetration depth of the ball inside the liner is δ as illustrated in Fig. 1. The vector that connects the point O_c to the point O_b is described as the eccentricity vector. The normal and tangential directions at the contact point are defined by $\mathbf{n}$ and $\mathbf{t}$ which are unit vectors in the direction of the clearance vector and tangential relative velocity at the contact point. In the Cartesian right-hand coordinate system illustrated in Fig. 1, the x axis points from the lateral to the medial direction (L–M); the z axis points from inferior to superior and the y axis parallel and in the walking direction from posterior to anterior (P–A). Moreover, the cup is considered to be stationary and anatomically inclined from the horizontal plane around y axis with an angle of $\pi/4$.

The following are some of the most relevant kinematics aspects related to the spherical clearance joint. In a spherical coordinate system, orthogonal unit vectors $(\mathbf{e}_r, \mathbf{e}_\theta, \mathbf{e}_\varphi)$ can be expressed as follow

$$\begin{aligned}\mathbf{n} = \mathbf{e}_r &= \sin\varphi\cos\theta\mathbf{i} + \sin\varphi\sin\theta\mathbf{j} + \cos\varphi\mathbf{k}\\ \mathbf{e}_\theta &= -\sin\theta\mathbf{i} + \cos\theta\mathbf{j} + 0\mathbf{k}\\ \mathbf{e}_\varphi &= \cos\varphi\cos\theta\mathbf{i} + \cos\varphi\sin\theta\mathbf{j} - \sin\varphi\mathbf{k}.\end{aligned} \tag{1}$$

The evaluation of the normal contact and tangential friction forces requires the computation of relative tangential and normal velocities of contact points on the head and cup surfaces. Therefore, position vectors of contact points can be written as follows

$$\mathbf{r}_{P_b} = \mathbf{r}_{O_b} + \mathbf{r}_{P_b/O_b}, \tag{2}$$

$$\mathbf{r}_{P_c} = \mathbf{r}_{P_c/O_c}, \tag{3}$$

in which $\mathbf{r}_{P_b}$ and $\mathbf{r}_{P_c}$ are the position vectors of contact points on the head and cup with respect to the global reference frame placed at the centre of the cup, O_c. The distance vector between the contact points of the cup and head is given by

$$\mathbf{r}_{P_b/P_c} = \mathbf{r}_{O_b} + \mathbf{r}_{P_b/O_b} - \mathbf{r}_{P_c/O_c}, \tag{4}$$

where

$$\mathbf{r}_{O_b} = r\mathbf{n}, \tag{5}$$

which is the eccentricity vector. Differentiating Eq. (4) with respect to time yields

$$\begin{aligned}\mathbf{v}_{P_b/P_c} = \frac{\mathrm{d}}{\mathrm{d}t}\left(\mathbf{r}_{P_b/P_c}\right) &= \frac{\mathrm{d}}{\mathrm{d}t}\left(r\mathbf{n}\right)\\ &+ \boldsymbol{\Omega}_b \times \mathbf{r}_{P_b/O_b} - \boldsymbol{\Omega}_c \times \mathbf{r}_{P_c/O_c},\end{aligned} \tag{6}$$

where

$$\boldsymbol{\Omega}_b = \omega_x\mathbf{i} + \omega_y\mathbf{j} + \omega_z\mathbf{k}. \tag{7}$$

and $\boldsymbol{\Omega}_c$ is zero because the cup is assumed to be stationary. Furthermore, ω_x, ω_y and ω_z are angular velocities of the femoral head around the vectors x, y and z, respectively. Consequently, the relative velocity of contact points is written as

$$\mathbf{v}_{P_b/P_c} = \underbrace{\dot{r}\mathbf{n}}_{v_n\mathbf{n}} + \underbrace{\left(r\dot{\theta}\sin\varphi\mathbf{e}_\theta + r\dot{\varphi}\mathbf{e}_\varphi + \boldsymbol{\Omega}_b \times R_b\mathbf{n}\right)}_{v_t\mathbf{t}}, \tag{8}$$

in which **t** is the tangential unit vector at contact point and

$$\theta = \tan^{-1}(y/x), \tag{9}$$

$$\varphi = \tan^{-1}(\sqrt{x^2 + y^2}/z), \tag{10}$$

$$r = \sqrt{x^2 + y^2 + z^2}, \tag{11}$$

$$\dot{\theta} = \frac{\dot{y}x - \dot{x}y}{x^2 + y^2}, \tag{12}$$

$$\dot{\varphi} = \frac{zx\dot{x} + zy\dot{y} - \dot{z}x^2 - \dot{z}y^2}{r^2\sqrt{x^2 + y^2}}, \tag{13}$$

$$\dot{r} = \frac{x\dot{x} + y\dot{y} + z\dot{z}}{r}, \tag{14}$$

and R_b is the femoral head radius. Finally, the relative penetration depth, shown in Fig. 1, can be computed as

$$\delta = r - (R_\mathrm{c} - R_\mathrm{b}). \tag{15}$$

where $R_\mathrm{c} - R_\mathrm{b}$ is defined as joint radial clearance that is specified by the user.

Equation (8) represents the relative tangential and normal velocities of contact points locating on the femoral head and cup surfaces. These velocity components are used to compute normal and tangential contact forces on the collision plane which will be considered in the next subsections.

2.2 Normal contact force models

It has been recognised by many authors that modelling normal contact forces during impact plays a critical role in the dynamic response of mechanical systems. The contact force model must be evaluated using a suitable constitutive law that takes into account material properties of the colliding bodies, geometric characteristics of the impacting surfaces and the impact velocity. Additionally, the numerical method for the calculation of the contact forces should be stable in order to allow for the integration of the equations of motion [33–36]. While various types of constitutive laws have been published, the Hertzian model remains the most utilised [37]. The contact force between the femoral head and cup, represented by a sphere and a hemisphere, respectively, can be modelled by the Hertz contact law given as

$$\mathbf{F}^n_{p_j} = K\delta^n \mathbf{n}. \tag{16}$$

where K is the stiffness coefficient and δ is the relative penetration depth given by Eq. (15). In general, the exponent n is set to 1.5. However, this law is purely elastic in nature and cannot represent the energy loss during the impact process. Lankarani and Nikravesh [25] overcame this difficulty by separating the normal contact force into elastic and dissipative components,

$$\mathbf{F}^n_{p_j} = \left(K\delta^n + D\dot{\delta}\right)\mathbf{n}. \tag{17}$$

where D denotes damping coefficient of the impacting bodies. Utilizing Lankarani and Nikravesh model, the normal contact force developed on the head can be expressed as

$$\mathbf{F}^n_{p_j} = -K\delta^{\frac{3}{2}}\left(1 + \frac{3\left(1 - c_e^2\right)}{4}\frac{\dot{\delta}}{\dot{\delta}^{(-)}}\right)\mathbf{n}. \tag{18}$$

where $\dot{\delta}$ and $\dot{\delta}^{(-)}$ are the relative penetration velocity and the initial impact velocity, respectively, and c_e represents the coefficient of restitution which is a specified parameter. The generalised stiffness parameter K depends on the geometry and physical properties of the contacting surfaces, which for two spherical contacting bodies with radii R_i and R_j are expressed by [37]

$$K = \frac{4}{3\left(\sigma_i + \sigma_j\right)}\left(\frac{R_i R_j}{R_i - R_j}\right)^{1/2}. \tag{19}$$

in which the material parameters σ_i and σ_j are given by

$$\sigma_z = \frac{1 - \upsilon_z^2}{E_z}. \tag{20}$$

where E and υ are Young's modulus and Poisson's ratio, respectively. It must be highlighted that the use of Eq. (18) is limited by Love's criterion, that is, it is only valid for impact velocities lower than the propagation velocity of elastic waves across the bodies [38].

It must be stated that there are other contact force models that can be utilised in multibody system contact problems. In particular, the interested reader can find relevant information on the impact between spheres in the publications by Machado et al. [39].

2.3 Tangential contact force

When two surfaces enter into contact phase and tend to slide against each other, friction develops and acts as a resistance to the relative motion. According to Eq. (8), which represents the relative velocity of contact points, the tangential force due to friction phenomenon has to be considered when the relative velocity has a relative tangential velocity component. Moreover, friction

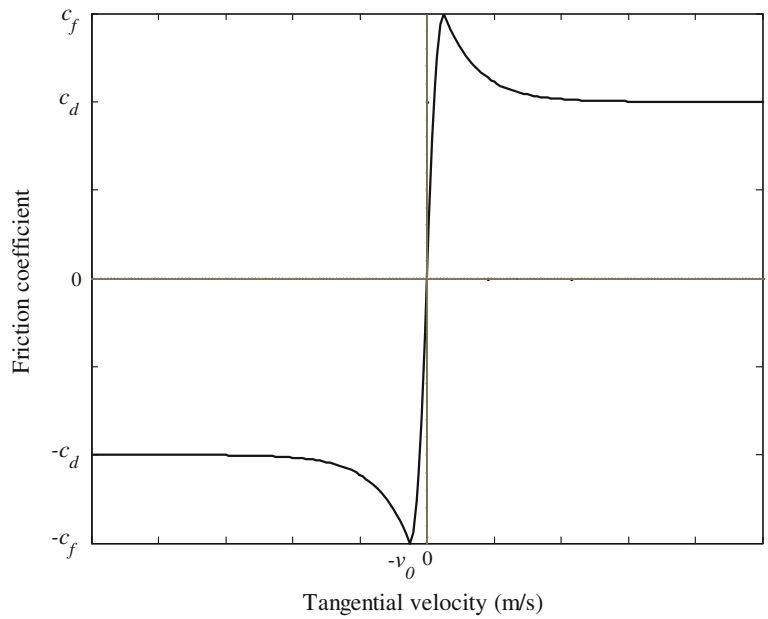

Fig. 2 Friction coefficient characteristic [24]

force acts like a cross-coupling force linking normal and parallel motions at the contact surface [11]. The most commonly used friction model is the Coulomb law which assumes the tangential friction force is proportional to the normal contact force. This model does not, however, explain neither the stick–slip phenomenon nor the negative damping effect [40]. Therefore, a model which can provide a good representation of the friction between sliding surfaces, while taking into account stick–slip and negative damping effect should be employed. The tangential contact forces can be evaluated as friction force using a modified Coulomb friction law [41]

$$\mathbf{F}^t_{p_j} = -\mu\left(v_t\right)\left\|\mathbf{F}^n_{p_j}\right\|\mathbf{t}, \tag{21}$$

where v_t represents the tangential velocity and μ denotes the friction coefficient. The friction force defined in Eq. (21) also permits the friction force to follow the displacement and act as a follower force. Although this coefficient depends on a number of parameters, the model used in the present study is confined to dependence on the relative velocity between the head and cup only. Therefore, the following friction function is generated

$$\mu\left(v_t\right) = \begin{cases} \left(-\frac{c_f}{v_0^2}\left(|v_t| - v_0\right)^2 + c_f\right)\operatorname{sgn}\left(v_t\right), \\ \quad |v_t| < v_0 \\ \left(c_d + \left(c_f - c_d\right)\exp\left(-\xi\left(|v_t| - v_0\right)\right)\right)\operatorname{sgn}\left(v_t\right), \\ \quad |v_t| \geq v_0 \end{cases} \tag{22}$$

The first part of the friction coefficient function uses a near zero continuous curve to avoid divergence of the numerical model. The second term is the Stribeck friction relation in which c_f and c_d are related to static and dynamic friction coefficients, respectively. In addition, $\xi > 0$ is the negative slope of sliding state [42] and v_0 is velocity tolerance that is defined to avoid computational instability as the change of velocity direction. This friction coefficient function is represented in Fig. 2. After friction coefficient starts from zero, it increases to peak friction which Bengisu and Akay [24] referred as static friction, c_f. The friction coefficient then reduces with increasing tangential velocity until the friction finally reaches steady state.

2.4 Dynamic governing equations of the system

In this subsection, governing equations of system motion are derived, based on the free body diagram of the femoral head illustrated in Fig. 3. The rotation of the femoral head around the x, y and z axes, represents flexion–extension (FE), abduction–adduction (AA) and internal–external rotation (IER), respectively. The normal contact and friction forces are computed according to the constitutive laws presented above and then transferred to the head centre. Thus, employing Newton's Second law yields

$$\sum M_{Ox} = I\ddot{\beta}_x, \sum M_{Ox} = M_{xx} - \left(R_j\mathbf{n} \times \mathbf{F}^t_{p_j}\right)\cdot\mathbf{i}\,\langle\delta\rangle^0$$

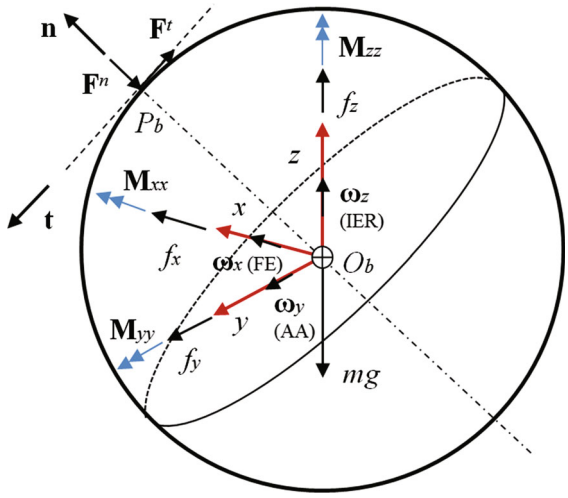

Fig. 3 Free body diagram of the femoral head

$$\sum M_{Oy}=I\ddot{\beta}_y,\ \sum M_{Oy}=M_{yy}-(R_j\mathbf{n}\times\mathbf{F}^t_{p_j})\cdot\mathbf{j}\,\langle\delta\rangle^0$$
$$\sum M_{Oz}=I\ddot{\beta}_z,\ \sum M_{Oz}=M_{zz}-(R_j\mathbf{n}\times\mathbf{F}^t_{p_j})\cdot\mathbf{k}\,\langle\delta\rangle^0, \tag{23}$$

$$\sum F_X=m\ddot{x},\ \sum F_X=f_x+\left(\mathbf{F}^t_{p_j}+\mathbf{F}^n_{p_j}\right)\cdot\mathbf{i}\,\langle\delta\rangle^0$$
$$\sum F_Y=m\ddot{y},\ \sum F_Y=f_y+\left(\mathbf{F}^t_{p_j}+\mathbf{F}^n_{p_j}\right)\cdot\mathbf{j}\,\langle\delta\rangle^0$$
$$\sum F_Z=m\ddot{z},\ \sum F_Z=f_z+\left(\mathbf{F}^t_{p_j}+\mathbf{F}^n_{p_j}\right)\cdot\mathbf{k}\,\langle\delta\rangle^0-mg. \tag{24}$$

Since the rotation angle of femoral head and its first and second derivations are known, then the angular momentum can be determined in order to obtain the external moment vector, **M**, which acts at the ball centre to result in the known angular acceleration.

$$\mathbf{M}=\mathrm{I}\ddot{\boldsymbol{\beta}}+R_j\mathbf{n}\times\mathbf{F}^t_{p_j}\,\langle\delta\rangle^0, \tag{25}$$

where

$$\mathbf{M}=\begin{pmatrix}M_{xx}\\M_{yy}\\M_{zz}\end{pmatrix},\quad \ddot{\boldsymbol{\beta}}=\begin{pmatrix}\ddot{\beta}_x\\\ddot{\beta}_y\\\ddot{\beta}_z\end{pmatrix}, \tag{26}$$

and $\langle\delta\rangle^0$ is discontinuity function defined as

$$\langle\delta\rangle^0=\begin{cases}1 & \delta>0\\ 0 & \delta\le 0.\end{cases} \tag{27}$$

in which $\delta>0$ represents when the system is in contact and $\delta\le 0$ for free flight mode. The normal and tangential contact forces are only effective if the system is in contact mode, which means detecting impact is an important step [43]. Moreover, the impact and rebound velocities and location should be obtained as initial conditions for solving motion equations of following dynamic scenario, which are either free flight or contact mode. In order to detect either impact or rebound time, the following condition should be assessed during the solution process by progressing time:

$$\delta\left(t^i\right)<0,\quad \delta\left(t^{i+1}\right)>0, \tag{28}$$

Finally, the equations of motion can be written as

$$\begin{bmatrix}m&0&0\\0&m&0\\0&0&m\end{bmatrix}\begin{bmatrix}\ddot{x}\\\ddot{y}\\\ddot{z}\end{bmatrix}=\begin{bmatrix}f_x+\left(\mathbf{F}^t_{p_b}+\mathbf{F}^n_{p_b}\right)\cdot\mathbf{i}\,\langle\delta\rangle^0\\ f_y+\left(\mathbf{F}^t_{p_b}+\mathbf{F}^n_{p_b}\right)\cdot\mathbf{j}\,\langle\delta\rangle^0\\ f_z+\left(\mathbf{F}^t_{p_b}+\mathbf{F}^n_{p_b}\right)\cdot\mathbf{k}\,\langle\delta\rangle^0-mg\end{bmatrix} \tag{29}$$

Using the state space representation, the second order equations of motion, Eq. (29) can be rewritten as a first order equations set as

$$\dot{\mathbf{z}}=\mathbf{H}\left(\mathbf{z}\right), \tag{30}$$

where $\mathbf{z}=\left[z_1\ z_2\ z_3\ z_4\ z_5\ z_6\right]^T=\left[x\ y\ z\ \dot{x}\ \dot{y}\ \dot{z}\right]^T$ and $\mathbf{H}(\mathbf{z})$ is given as follows

$$\dot{\mathbf{z}}=\begin{bmatrix}\dot{z}_1\\\dot{z}_2\\\dot{z}_3\\\dot{z}_4\\\dot{z}_5\\\dot{z}_6\end{bmatrix}=\frac{1}{m}\begin{bmatrix}z_3\\z_4\\z_5\\f_{z_1}+\left(F^t_{p_b}+F^n_{p_b}\right)\cdot\mathbf{i}\,\langle\delta\rangle^0\\ f_{z_2}+\left(F^t_{p_b}+F^n_{p_b}\right)\cdot\mathbf{j}\,\langle\delta\rangle^0\\ f_{z_3}+\left(F^t_{p_b}+F^n_{p_b}\right)\cdot\mathbf{k}\,\langle\delta\rangle^0-mg\end{bmatrix} \tag{31}$$

In turn, r, θ, φ and their time derivatives can be expressed with respect to state space parameters in Eq. (31). The resulting equations are nonlinear and must be solved by using a numerical method. In the present work, the adaptive Runge-Kutta-Fehlberg method is utilised to discretise the interval of time [44]. In the next section, the results of solutions for Eq. (31) for artificial hip joints will be presented and discussed.

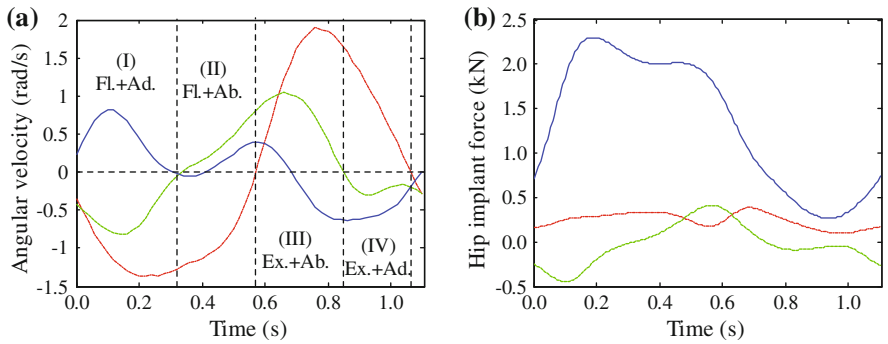

Fig. 4 **a** Angular velocities where—ω_z(IER); *dashed lines* ω_y(AA); *dashed dotted lines* ω_x(FE); **b** Physiological adopted forces with—f_z(Vertical); *dashed lines* f_y(A-P); *dashed dotted lines* f_x(M-L) for the gait cycle

3 Results and discussion

In this section, the governing motion equations of a CoC artificial hip joint with clearance are solved. The ceramic components are represented with the following material properties: 3.58e11 GPa Young's modulus, 0.23 Poisson's ratio and 4370 kg/m^{3}density. The hip implant is modelled as a joint with a clearance size of 50 μm and restitution coefficient 0.9, while friction coefficients are assumed to be C_f / C_d=0.15 / 0.1. Three-dimensional physiological forces and angular velocities were sourced from the literature and shown in Fig. 4a, b [45]. The dynamic response of the system is obtained by solving the equations of motion using the adaptive Runge-Kutta–Fehlberg method. The computational method is stable and solutions to the equations are always achieved. Moreover, total computation time for the present method is no longer than 20 min.

3.1 Contact point path

The contact point track between the femoral head and cup over the gait cycle has a significant influence on the computed wear rates as observed in Archard's wear methodology [14]. Moreover, establishing near physiological motion in a joint simulator is of paramount importance when understanding wear rates [21]. Owing to the crucial significance of contact point tracking and wear, this section aims to dynamically study the path of contact point between the femoral head and cup with both low and high friction in a non-lubricated joint.

In the first comparison, the sliding track of a specific point on the femoral head surface is demonstrated against the path of contact point between the femoral head and cup. This sliding track is shown as continuous blue line in Fig. 5a and is calculated based on the computational method proposed by Saikko and Calonius [21]. While the contact point path of frictionless head/cup articulation is drawn in Fig. 5a as a distinct red line. The specific point coincides with the contact point when the heal strikes, shown by the square in Fig. 5a. Moreover, these two curves cross each other five points despite the starting point (square point). However, curves pass through those cross points at different times as stated in the figure and its caption. The sliding distances of both curves are illustrated in Fig. 5b. It can be concluded that sliding distance obtained from the

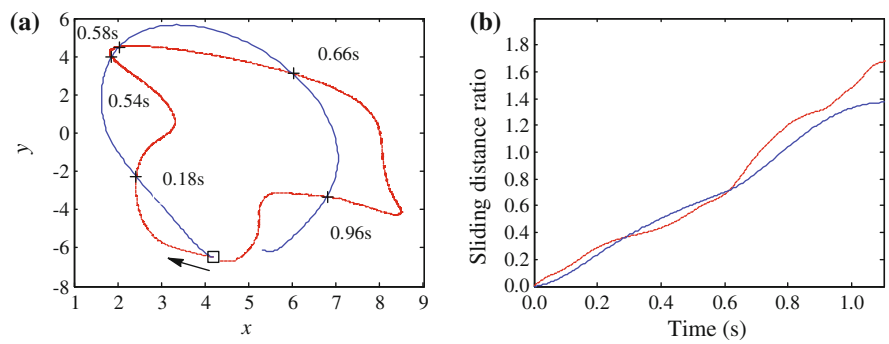

Fig. 5 **a** Sliding track of the *square point* and contact track point of artificial hip joint, (times in which the continuous *blue curve* passes the cross points are 0.1986, 0.4469, 0.4744, 0.6068 and 0.9158s, respectively), **b** corresponding sliding distances. (Color figure online)

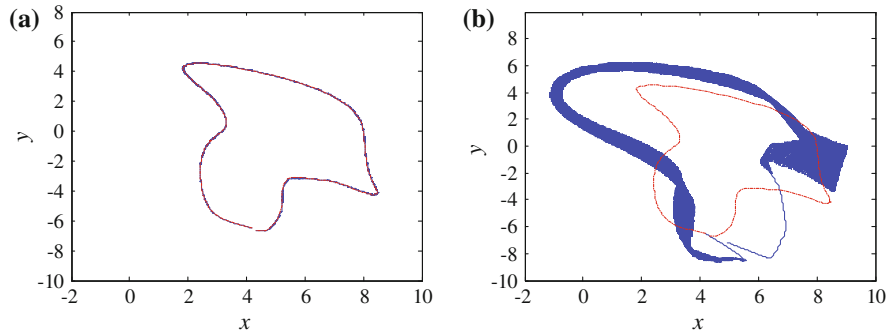

Fig. 6 The track of contact point projected on $x - y$ surface. **a** contact point tracks obtained from an ideal joint (*distinct red line*) and clearance joint with low friction coefficient (*continuous blue line*), **b** contact point tracks acquired from an ideal joint (*distinct red line*) and clearance joint with high friction coefficient (*continuous blue line*). (Color figure online)

present method for contact point track is very close to that acquired from Saikko and Calonius [21].

There is a strong analogy between the contact point path computed by the present multibody dynamic approach for an ideal and low friction artificial hip joint. Assuming the hip implant is ideal without both clearance and friction, the contact point track between the head and cup can be calculated by knowing the contact point where is on the head surface and the direction of the forces acting at the femoral head centre, shown in Fig. 6a as distinct red lines. The continuous blue line is obtained from the present method for a clearance joint assuming the friction is very low. The track of contact point is very close to that of an ideal joint, as seen in Fig. 6a. This result is consistent with the sliding track used by Raimondi et al. [18] and Mattei et al. [17]. They assumed the reaction force between the head and cup lays in the direction joining their centres due to the frictionless contact. Interestingly, the contact point track of a hip implant with high friction differs considerably from the ideal and low friction modes as observed in Fig. 6b. It can be drawn that the contact point of the system with high friction over the gait cycle moves a longer length from the start to end point of the track than that with the low friction case. Consequently, the alteration in motion will affect implant wear and deformation rates over the long term. Another significant difference as a result of increased friction is the oscillatory behaviour of the head motion inside the cup observable as thick path lines (Fig. 6b). This vibrational motion of the femoral head inside the cup has to be taken into account when evaluating wear rates, since the location of contact point changes repeatedly even though with an amplitude in very minute fashion. According to both the increase of sliding distance and oscillatory movement of the femoral head, it is hypothesised that wear rates can become greater.

3.2 Hip squeaking

A FFT frequency analysis of the audible sounds from the head centre acceleration was also carried out to assess the frequency of hip squeaking. Fundamental hip squeaking frequencies of artificial hip joints with different cup radii are plotted in Fig. 7. Results are consistent with those found in vivo by Walter et al. [2] which are in the range of 400–7500 Hz. Hip squeaking frequencies were found to increase as hip implant size decreases. Moreover, it was found that CoC artificial hip joints do not squeal when the friction is below a critical value [46].

3.3 Three-dimensional vibration

In this subsection, vibrations of the femoral head inside the cup are investigated. Recently, Weiss et al. [9] showed the femoral head vibrates inside the cup with two-dimensional micrometre movement. However, they did not report any vibration of the ball in the third dimension, that being the normal z direction. The present paper aims to provide a better understanding of the three-dimensional vibration of the femoral head inside the socket. Trajectory of the femoral head in planes $x - y$, $x - z$ and $y - z$ is shown in Fig. 8a–c.

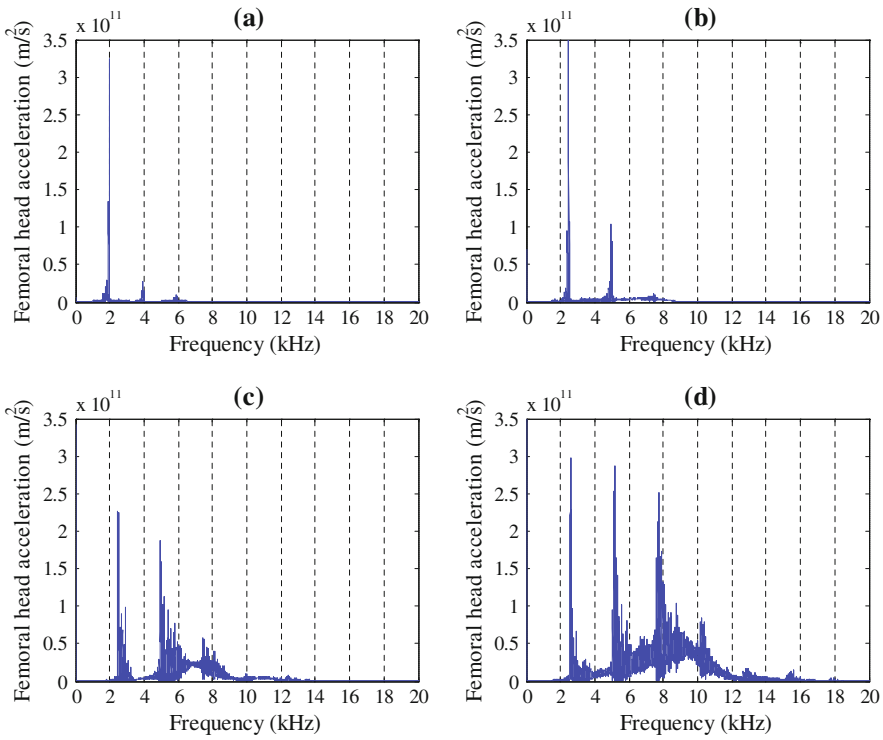

Fig. 7 FFT analysis of CoC hip implants for different cup radii. **a** 25 mm; **b** 20 mm; **c** 16 mm; **d** 14 mm

The thickness of the contact point track demonstrates the vibration of the femoral head inside the cup. In order to better understand the ball vibration, two different instants of the gait cycle are selected arbitrary, namely t = 0.5 and 0.7 s and the ball vibration in different planes is shown in Fig. 8 at those instants. Figure 8a-1, a-2 are consistent with results found experimentally by Weiss et al. [9] in 2D. They reported a micrometre scale elliptical motion of the ball inside the liner and determined the cause of squeaking is mode-coupling instability. In addition, the femoral head vibrates in all three directions x, y and z, as shown in Fig. 8b-1, b-2, c-1, c-2. The amplitude of ball vibration in z direction is very small compared to the x and y directions.

In addition to mode-coupling instability, the orientation of the femoral head motion changes significantly during the gait cycle. The friction force which is a non-conservative force alters its direction to track the ball displacements. This force is a follower force and leads the system to friction-induced vibration. Follower forces are well-known sources of asymmetry in stiffness matrices and are considered to be responsible for flutter instabilities in a wide variety of mechanical systems [47].

3.4 stick–slip and negative damping

When the relative tangential speed between the femoral head and cup at the contact point is very low, stick–slip phenomenon arises because of the difference between static and kinetic friction. Moreover, there is a negative friction–velocity gradient as observed in Fig. 2, which leads to friction-induced vibration by introducing a negative damping component in the equations of motion. Figure 9 illustrates stick and slip phase intervals of the ball motion during a normal walking cycle. The goal in this section is considering if stick–slip friction and negative damping effect are causes of the femoral head vibration. The plot can be categorised by three phases, namely stick, stick–slip and pure slip. In the quasi-static stick phase, friction lies on the very steep, negative-sloping region of the friction curve. The femoral head goes from stick to slip and vice versa repeatedly in the stick–slip region, which induces the system to vibrate. During the slip part, the system can also undergo friction-induced vibration owing to negative-sloping velocity as the velocity increases which lead to a negative damping component in the equations of motion.

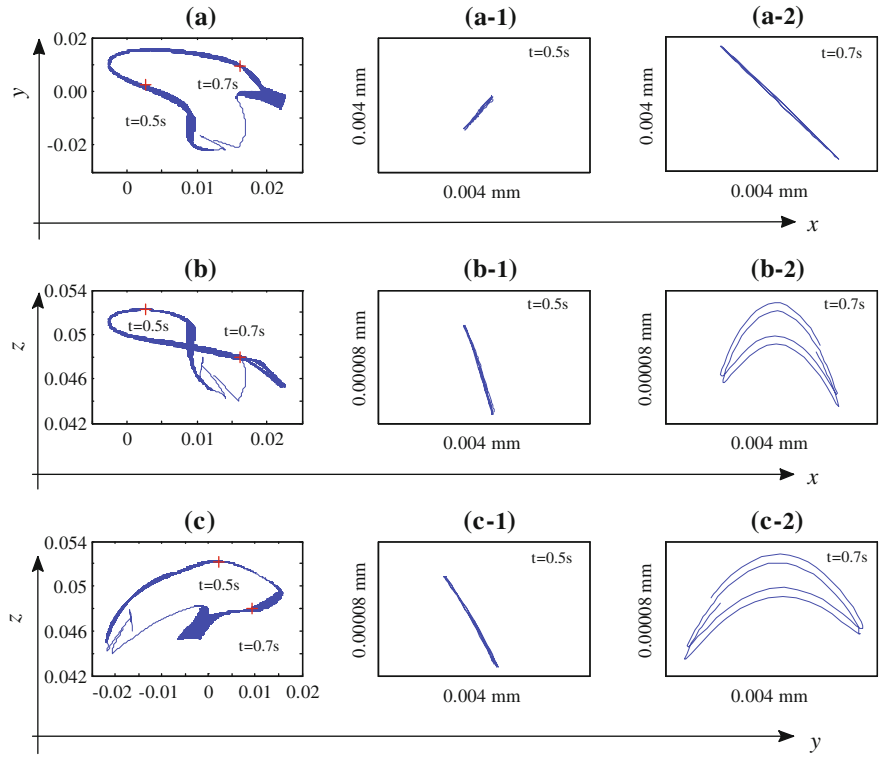

Fig. 8 Contact point track and the vibration of the femoral head in x, y and z directions

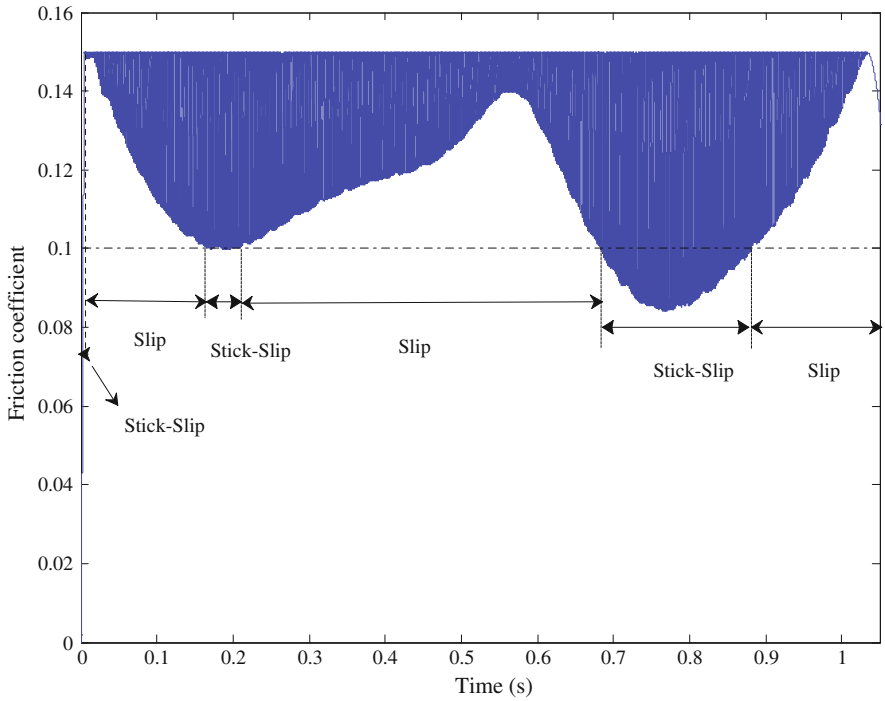

Fig. 9 *Stick and slip phase* intervals over one normal walking cycle

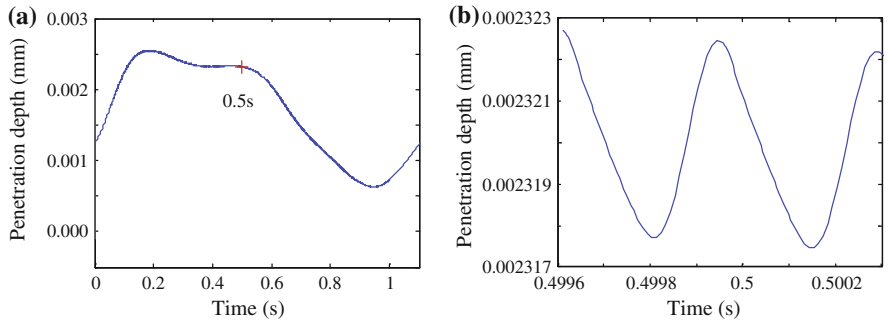

Fig. 10 Penetration depth during the gait cycle (**a**) and the oscillation of indentation close $t = 0.5$ s

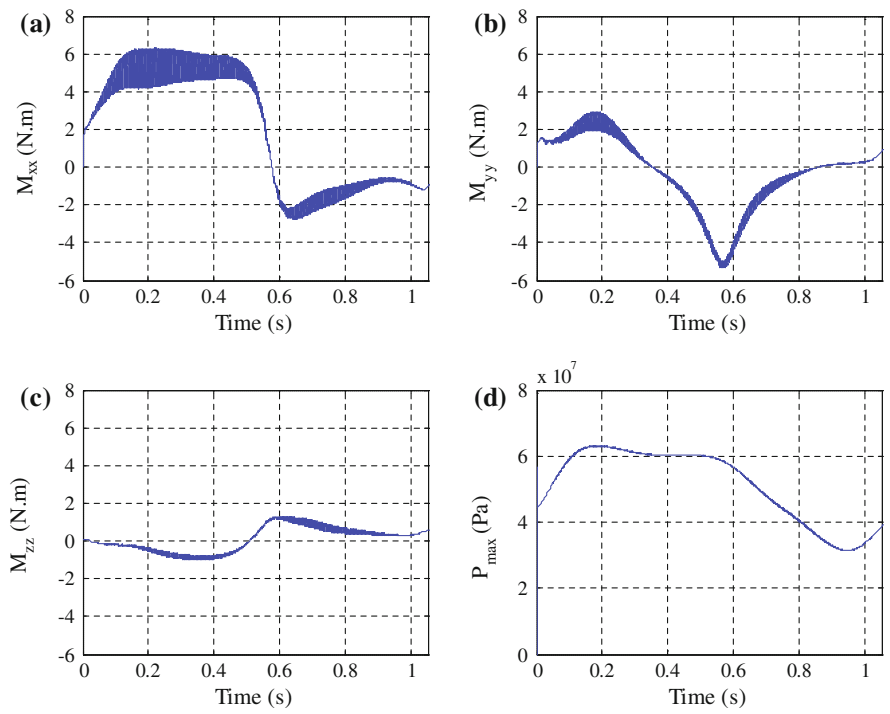

Fig. 11 The femoral head moments and maximum contact stress of an artificial hip joint with friction

3.5 Normal contact force changes

Figure 10a shows penetration depth with respect to time during the gait cycle, while Fig. 10b depicts oscillatory trend of penetration depth at a time of 0.5 s. This section considers friction-induced vibration due to contact force changes shown in Fig. 11d. It can be seen in Fig. 10b that the indentation of the head into the cup surfaces has a vibrational behaviour due to alteration in the contact force. Such a vibration is harmonic with frequency in the audible range of 2800 Hz at $t = 0.5$ s. Consequently, the friction-induced vibration occurs in artificial hip joints due to contact force changes and the corresponding frequencies are in the audible range. There is neither high increase contact force nor decrease penetration depth according to Figs. 10a and 11d, so the system does not undergo sprag-slip. Moreover, penetration depth is not zero or negative which means the femoral head remains in contact during the gait cycle.

3.6 Hip implant moments and contact stress

The contact stresses and contact area between the femoral head and cup of artificial hip joints are key determinants of implant wear. Furthermore, artificial hip joint moments due to friction and joint kinetics, may induce prosthetic implant loosening. This subsection aims to investigate the effect of friction-induced vibration on maximum contact pressure and moments of

CoC artificial hip joints. The effect of friction-induced vibration is considered on moments and contact stress of artificial hip joint over the gait cycle in Fig. 11. As can be seen from the wide lines in the plot, friction-induced vibration leads to an oscillatory behaviour in the moment and contact stress curves. This demonstrates that friction-induced vibration of the femoral head moving against the liner does significantly alter the amplitude of moment and contact stress oscillation within the joint. As variation in these parameters directly influences prosthetic wear, and maybe loosening, these characteristics should be taken into account during implant design. Moreover, the oscillating trend of moments and contact stress during the gait cycle can affect rehabilitation after total hip replacement.

4 Conclusion

Hip squeaking and the path of contact point between the head and cup of a CoC hip implant were investigated using a spatial multibody dynamic model. The approach took not only tribological properties of bearing surfaces, but also three-dimensional physiological hip joint gait motions into account to derive and solve nonlinear equations of motion. Furthermore, it was robust and fast with respect to computation time. Results were verified by comparing with in vivo, experimental and computational outcomes available in the literature.

It was be concluded that hip implant vibration resulted from stick–slip, mode-coupling, contact force changes and negative damping in the system. It was also shown that the vibration of an artificial hip joint had a three-dimensional characteristic. Vibration amplitude of the femoral head in Z-direction was much lower than the X and Y directions. Friction-induced vibration induced considerable oscillatory behaviour in the X, Y and Z moments of the hip implant. Hip squeaking frequencies increased with decreasing hip implant size. Finally, it was illustrated that friction resulted in an alteration in the contact point track as well as vibration of the femoral head inside the cup. This can increase the sliding distance, which significantly affects wear in artificial hip joints.

Acknowledgments The first author gratefully acknowledges Macquarie University for International Macquarie University Research Excellence Scholarship (iMQRES)—No. 2010017. The second author expresses his gratitude to the Portuguese Foundation for the Science and Technology under the research Project BIOJOINTS (PTDC/EME-PME/099764/2008).

References

1. Restrepo, C., Parvizi, J., Kurtz, S., Sharkey, P., Hozack, W., Roth-man, R.: The noisy ceramic hip: is component malpositioning the cause? J. Arthroplast. **23**, 643–649 (2008)
2. Walter, W., Waters, T., Gillies, M., Donohoo, S., Kurtz, S., Ranawat, A., Hozack, W., Tuke, M.: Squeaking hips. J. Bone Joint Surg Am **90**(4), 102–111 (2008)
3. Rieker, C., Köttig, P., Schön, R., Windler, M., Wyss, U.: Clinical wear performance of metal-on-metal hip arthroplasties J.J. Jacobs, T.L. Craig (Eds.), Alternative Bearing Surfaces in Total Joint Replacement. ASTM STP 1346, American Society for Testing and Materials (1998)
4. Currier, J., Anderson, D., Van Citters, D.: A proposed mechanism for squeaking of ceramic-on-ceramic hips. Wear **269**, 782–789 (2010)
5. Weiss, C., Hothan, A., Morlock, M.M., Hoffmann, H.: Friction-induced vibration of artificial hip joints. GAMM-Mitteilungen **32**(2), 193–204 (2009)
6. Weiss, C., Gdaniec, P., Hoffmann, N.P., Hothan, A., Huber, G., Morlock, M.M.: Squeak in hip endoprosthesis systems: an experimental study and a numerical technique to analyze design variants. Med. Eng. Phys. **32**, 604–609 (2010)
7. Fan, N., Chen, G., Qian, L.: Analysis of squeaking on ceramic hip endoprosthesis using the complex eigenvalue method. Wear **271**, 2305–2312 (2011)
8. Fan, N., Chen, G.: Numerical study of squeaking suppresses for ceramic-on-ceramic hip endoprosthesis. Tribol Int **48**, 172–181 (2012)
9. Weiss, C., Hothan, A., Huber, G., Morlock, M., Hoffmann, N.: Friction-induced whirl vibration: root cause of squeaking in total hip arthroplasty. J. Biomech. **45**, 297–303 (2012)
10. Akay, A.: Acoustics of friction. J. Acoust. Soc. Am. **111**(4), 1525–1548 (2002)
11. Hoffmann, N., Fischer, M., Allgaier, R., Gaul, L.: A minimal model for studying properties of the mode-coupling type instability in friction induced oscillations. Mech. Res. Commun. **29**, 197–205 (2002)
12. Popp, K., Stelter, P.: Stick-slip and chaos. Philos. Trans. R. Soc. Lond. A **332**, 89–105 (1990)
13. Kinkaid, N.M., O'Reilly, O.M., Papadopoulos, P.: Automotive disc brake squeal. J. Sound Vib. **267**, 105–166 (2003)
14. Archard, J.F.: Contact and rubbing of flat surfaces. J. Appl. Phys. **24**, 981–988 (1953)
15. Barbour, P.S.M., Stone, M.H., Fisher, J.: A hip joint simulator study using simplified loading and motion cycles generating physiological wear paths and rates. Proc. Inst. Mech. Eng. Part H **213**(6), 455–467 (1999)
16. Saikko, V., Calonius, O., Kernen, J.: Effect of slide track shape on the wear of ultra-high molecular weight polyethylene in a pin-on-disk wear simulation of total hip prosthesis. J. Biomed. Mater. Res. Part B **69 B**(2), 141–148 (2004)
17. Mattei, L., Di Puccio, F., Ciulli, E.: A comparative study of wear laws for soft-on-hard hip implants using a mathematical wear model. Tribol. Int. **63**, 66–77 (2013)

18. Raimondi, M.T., Santambrogio, C., Pietrabissa, R., Raffelini, F., Molfetta, L.: Improved mathematical model of the wear of the cup articular surface in hip joint prostheses and comparison with retrieved components. Proc. Inst. Mech. Eng. Part H **215**(4), 377–391 (2001)
19. Jourdan, F., Samida, A.: An implicit numerical method for wear modeling applied to a hip joint prosthesis problem. Comput. Methods Appl. Mech. Eng. **198**, 2209–2217 (2009)
20. Ramamurti, B., Bragdon, C.R., O'Connor, D.O., Lowenstein, J.D., Jasty, M., Estok, D.M., Harris, W.H.: Loci of movement of selected points on the femoral head during normal gait: three-dimensional computer simulation. J. Arthroplast. **11**(7), 845–852 (1996)
21. Saikko, V., Calonius, O.: Slide track analysis of the relative motion between femoral head and acetabular cup in walking and hip simulator. J. Biomech. **35**(4), 455–464 (2002)
22. Sariali, E., Stewart, T., Jin, Z., Fisher, J.: Three-dimensional modelling of in vitro hip kinematics under micro-separation regime for ceramic on ceramic total hip prosthesis: an analysis of vibration and noise. J. Biomech. **43**, 326–333 (2010)
23. Askari, E., Flores, P., Dabirrahmani, D., Appleyard, R.: Study of the friction-induced vibration and contact mechanics of artificial hip joints. Tribol. Int. **70**, 1–10 (2014)
24. Bengisu, M.T., Akay, A.: Stability of friction-induced vibrations in multi-degreeof-freedom systems. J. Sound Vib. **171**, 557–570 (1994)
25. Lankarani, H., Nikravesh, P.: A contact force model with hysteresis damping for impact analysis of multibody systems. J. Mech. Des. **112**, 369–376 (1990)
26. Flores, P., Lankarani, H.M.: Spatial rigid-multi-body systems with lubricated spherical clearance joints: modeling and simulation. Nonlinear Dyn. **60**, 99–114 (2010)
27. Brutti, C., Coglitore, C., Valentini, P.P.: Modeling 3D revolute joint with clearance and contact stiffness. Nonlinear Dyn. **66**(4), 531–548 (2011)
28. Tian, Q., Liu, C., Machado, M., Flores, P.: A new model for dry and lubricated cylindrical joints with clearance in spatial flexible multibody systems. Nonlinear Dyn. **64**, 25–47 (2011)
29. Flores, P., Koshy, C.S., Lankarani, H.M., Ambrósio, J., Claro, J.C.P.: Numerical and experimental investigation on multibody systems with revolute clearance joints. Nonlinear Dyn. **65**(4), 383–398 (2011)
30. Liu, C., Tian, Q., Hu, H.: Dynamics and control of a spatial rigid-flexible multibody system with multiple cylindrical clearance joints. Mech. Mach. Theory **52**, 106–129 (2012)
31. Flores, P., Lankarani, H.M.: Dynamic response of multibody systems with multiple clearance joints. J. Comput. Nonlinear Dyn. **7**(3), 031003 (2012). 13p
32. Muvengei, O., Kihiu, J., Ikua, B.: Numerical study of parametric effects on the dynamic response of planar multi-body systems with differently located frictionless revolute clearance joints. Mech. Mach. Theory **53**, 30–49 (2012)
33. Flores, P.: Modeling and simulation of wear in revolute clearance joints in multibody systems. Mech. Mach. Theory **44**(6), 1211–1222 (2009)
34. Silva, P.C., Silva, M.T., Martins, J.M.: Evaluation of the contact forces developed in the lower limb/orthosis interface for comfort design. Multibody Syst. Dyn. **24**, 367–388 (2010)
35. Lopes, D.S., Silva, M.T., Ambrósio, J.A., Flores, P.: A mathematical framework for contact detection between quadric and superquadric surfaces. Multibody Syst. Dyn. **24**(3), 255–280 (2010)
36. Flores, P., Machado, M., Silva, M.T., Martins, J.M.: On the continuous contact force models for soft materials in multibody dynamics. Multibody Syst. Dyn. **25**(3), 357–375 (2011)
37. Hertz, H.: Über die Berührung fester elastischer Körper. J. reine angewandte Mathematik **92**, 156–171 (1881)
38. Love, A.: A Treatise on the Mathematical Theory of Elasticity, 4th edn. Dover Publications, New York (1944)
39. Machado, M., Moreira, P., Flores, P., Lankarani, H.M.: Compliant contact force models in multibody dynamics: evolution of the Hertz contact theory. Mech. Mach. Theory **53**, 99–121 (2012)
40. Flores, P., Leine, R., Glocker, C.: Application of the nonsmooth dynamics approach to model and analysis of the contact–impact events in cam-follower systems. Nonlinear Dyn. **69**(4), 2117–2133 (2012)
41. Hetzler, H., Schwarzer, D., Seemann, W.: Analytical investigation of steady-state stability and Hopf-bifurcations occurring in sliding friction oscillators with application to low-frequency disc brake noise. Commun. Nonlinear Sci. Numer. Simul. **12**, 83–99 (2007)
42. Kanga, J., Krousgrilla, C.M., Sadeghi, F.: Oscillation pattern of stick-slip vibrations. Int. J. Non-linear Mech. **44**, 820–828 (2009)
43. Flores, P., Ambrósio, J.: On the contact detection for contact–impact analysis in multibody systems. Multibody Syst. Dyn. **24**(1), 103–122 (2010)
44. Atkinson, K.A.: An Introduction to Numerical Analysis, 2nd edn. Wiley, New York (1989)
45. Bergmann, G., Deuretzbacher, G., Heller, M., Graichen, F., Rohlmann, A., Strauss, J., et al.: Hip contact forces and gait patterns from routine activities. J. Biomech. **34**(7), 859–871 (2001)
46. Askari, E., Flores, P., Turner, D., Appleyard, R.: Planar multibody dynamic investigations of hip squeaking and ball trajectory in ceramic-on-ceramic artificial hip joints. In: VII Iberian Conference on Tribology. Porto, Portugal: FEUP (2013)
47. Guran, A., Pfeiffer, F., Popp, K.: (Eds), Dynamics with Friction: Modeling, Analysis and Experiment, Part II (Singapore: World Scientific) (2001)